7 Analysis of Neural Excitability and Oscillations

John Rinzel and Bard Ermentrout

7.1 Introduction

Qualitative features of excitable or oscillatory dynamics are shared by broad classes of neuronal models. Expressed in models for single-cell behavior as well as for ensemble activity, these features include excitability and threshold behavior; beating and bursting oscillations and phase locking; and bistability and hystersis. Our goal here is to illustrate, by exploiting a specific model of excitable membrane, some of the concepts and techniques that can be used to understand, predict, and interpret these dynamic phenomena biophysically. Our mathematical methods include numerical integration of the model equations, graphical or geometric representation of the dynamics (phase plane analysis), and analytic formulae for characterizing thresholds and stability conditions. The concepts are from the qualitative theory of nonlinear differential equations and nonlinear oscillations, and from perturbation and bifurcation theory. In this brief chapter, we will not consider the spatiotemporal aspects of distributed systems. Thus our methods apply directly only to a membrane patch, to a spatially uniform, equipotential cell, or to a network with each cell type perfectly synchronized.

Even seemingly simple models that exhibit one or two of the different dynamic behaviors, such as generation of individual or repetitive action potentials, may display a great variety of response characteristics when a broad range of parameters is considered. This means that a given cell or ensemble may behave in many different modes, for example, as a generator of single pulses, as a bursting pacemaker, as a bistable "plateauing" cell, or as a beating oscillator, depending upon the physiological conditions (neuromodulator or ionic concentrations) or stimulus presentations (applied currents or synaptic inputs). The nonlinear nature of the models provides the substrate for this broad repertoire; in contrast, linear models may be characterized by exponential or oscillatory time courses over their entire parameter ranges. It is important when studying a nonlinear model that stimulus-response properties be considered over ranges of the biophsical parameters.

In this chapter, we show that a simple, but biophysically reasonable, two-current excitable membrane model is sufficiently robust to exhibit such behavioral richness, as parameters are systematically varied. By adjusting channel densities, activation dynamics, and stimulus intensities, we find that the cell model can exhibit quite different threshold characteristics for spike generation (finite or infinite latency, with or without intermediate amplitude responses) and for onset of repetitive firing (finite or zero minimum frequency). The cell shows various types of bistable behavior: two

different rest states, in one case, and a rest state with a coexistent oscillatory response around a depolarized level, in another. The latter situation can provide a mechanism for rhythmic bursting when additional slower processes (e.g., slow channel kinetics, or a channel affected by slow ion accumulation) respond differently at the two potential levels. Because the spike-generating dynamics significantly influence the burst's waveform, there can be several different types of bursting depending on the nature of the fast dynamics; for example, parabolic bursting does not depend on bistability in the spike-generating processes. Finally, by considering the phase-resetting behavior for a self-oscillatory cell, we show that the response to a single brief, arbitrarily timed, perturbing stimulus can often be used to predict phase-locking responses to periodic stimulation, and to predict the synchronization properties of weakly coupled cells.

The underlying qualitative structure for these behaviors will be revealed with graphical phase plane analysis, complemented by a few analytic formulas. The concepts we will cover include steady states, trajectories, limit cycles, stability, domains of attraction, and bifurcation of solutions. Phase plane characteristics and system dynamics will be interpreted biophysically in terms of activation curves, current-voltage relations, and the like. A user-friendly program, XPP (developed by G. B. Ermentrout) for X-windows computers allows modelers to interactively generate, explore, and visualize most of the behaviors described here in the same spirit as an experimental "setup." (XPP's numerical procedures are summarized in chapter appendix B.) The concepts apply to higher-order systems, for which appropriate projections of phase space, motivated by differences in time scales for certain variables, can lead to similar insights.

7.2 Models for Excitable Cells and Networks

Most models for excitable membrane retain the general Hodgkin-Huxley (HH) format (Hodgkin and Huxley 1952), and can be written in the form

$$C\frac{dV}{dt} + I_{ion}(V, W_1, \ldots, W_n) = I(t) \tag{7.1}$$

$$\frac{dW_i}{dt} = \phi\frac{[W_{i,\infty}(V) - W_i]}{\tau_i(V)}, \tag{7.2}$$

where V denotes membrane potential (say, deviation from a reference, or "rest" level), C is membrane capacity, and I_{ion} is the sum of V- and t-dependent currents through the various ionic channel types; $I(t)$ is the applied current. The $W_i(t)$ vari-

ables describe the fraction of channels of a given type that are in various conducting states (e.g., open or closed) at time t. The first-order kinetics for W_i typically involve V dependence in the time constant τ_i; ϕ is a temperature-like time scale factor that may depend on i. If the current, I_j, for channel type j may be suitably modeled as ohmic, then it might be expressed as

$$I_j = \bar{g}_j \sigma_j(V, W_1, \ldots, W_n)(V - V_j), \tag{7.3}$$

where $\bar{g}_j$ is the total conductance with all j-type channels open (product of single-channel conductance with the total number of j channels), σ_j is the fraction of j channels that are open (it may depend on several of the W_i variables), and V_j is the reversal potential (usually Nernstian) for this ion species. For some channel types the current-voltage relation may be more appropriately represented by the Goldman-Hodgkin-Katz equation, or by a barrier kinetics scheme (Hille 1992), and the gating kinetics might involve a multistate Markov description. In the classical HH model (Hodgkin and Huxley 1952) for squid giant axon, there are three variables W_i, denoted as m, h, and n, to describe the fractions m^3h and n^4 of open Na^+ channels and K^+ channels, respectively.

For some purposes, it is important that the current balance equation (eq. 7.1) contain terms to account for ionic pump currents. These currents, as well as some channel conductances, may depend upon time-varying second messengers or ionic concentrations, for example, in diffusionally restricted intracellular or extracellular volumes. For such considerations, additional variables and transport or kinetic balance equations would be included in the model, and these will carry along their own time scales. Indeed, some models that include the dynamics of intracellular free calcium handling have assumed time constants that are orders of magnitude greater than channel kinetics and thereby set the time scale for phenomena such as bursting oscillations (see, for example, Chay and Keizer 1983). We also note that the form of eq. 7.2 is not unique; in a phenomenological model of Rall (see Goldstein and Rall 1974), the corresponding equations are nonlinear in the W_i.

Some models for excitability contain many variables and represent numerous channel types, especially models designed to account for rather detailed aspects of spike shape and dependence on many different pharmacological agents. On the other hand, if qualitative or semiquantitative characteristics of spike generation and input-output relations are adepuate, say in network simulations, then a reduced model having just a few variables may suffice. Such reductions can sometimes be obtained when time scale differences allow relatively fast variables to be instantaneously relaxed to pseudo–steady-state values; thus, if τ_j is small relative to other time constants, then one might set $W_j = W_{j,\infty}(V)$ in eq. 7.2. Likewise, functionally related

variables with similar time scales might be lumped together. In this spirit, FitzHugh (1960) considered reductions of the HH model (see also Rinzel 1985; Kepler, Abbott, and Marder 1992) and then introduced (FitzHugh 1961) and idealized, analytically tractable two-variable model (see also Nagumo, Arimoto, and Yoshizawa 1962) widely studied as a qualitative prototype for excitable systems in many biological and chemical contexts. A FitzHugh-Nagumo/Hodgkin-Huxley hybrid was formulated and studied by Morris and Lecar (1981), in the context of electrical activity of the barnacle muscle fiber. The model incorporates a V-gated Ca^{2+} channel and a V-gated, delayed-rectifier K^+ channel; neither current inactivates. A simple version of this model is represented by the equations

$$C\frac{dV}{dt} = -I_{ion}(V,w) + I \tag{7.4}$$

$$\frac{dw}{dt} = \phi\frac{[w_\infty(V) - w]}{\tau_w(V)}, \tag{7.5}$$

where

$$I_{ion}(V,w) = \bar{g}_{Ca}m_\infty(V)(V - V_{Ca}) + \bar{g}_K w(V - V_K) + \bar{g}_L(V - V_L). \tag{7.6}$$

In eqs. 7.4–7.6, w is the fraction of K^+ channels open, and the Ca^{2+} channels respond to V so rapidly that we assume instantaneous activation. One might introduce dimensionless variables, as in FitzHugh 1969 or Rinzel and Ermentrout 1989, in order (1) to reduce the number of free parameters and identify equivalent groups of parameters, and (2) identify and group "fast" and "slow" processes together. However, in the interest of clarity, we will keep all equations in their original form. In eq. 7.5, τ_w has been scaled so its maximum is now one, and ϕ equals the temperature factor divided by the prescaled maximum ($1/\sqrt{\lambda_w}$ in Morris and Lecar 1981). (The V-dependent functions, m_∞, w_∞, and τ_w, and the reference parameter sets are given in appendix A). All the computations and figures in this chapter are based on eqs. 7.4–7.6, and extensions of them for generating bursting behaviors.

Even network models in certain approximations can reduce to a few variables. One example is the Wilson-Cowan model (1972; for another, see chapter 11, this volume):

$$\mu_e\frac{d\mathscr{E}}{dt} = -\mathscr{E} + S(\alpha_{ee}\mathscr{E} - \alpha_{ie}\mathscr{I} - \theta_e) \tag{7.7}$$

$$\mu_i\frac{d\mathscr{I}}{dt} = -\mathscr{I} + S(\alpha_{ei}\mathscr{E} - \alpha_{ii}\mathscr{I} - \theta_i), \tag{7.8}$$

where $\mathscr{E}$ and $\mathscr{I}$ represent the respective firing rates of a population of excitatory and inhibitory interneurons. The parameters μ_e, μ_i are the membrane time constants; θ_e, θ_i are the firing thresholds; α_{ee}, α_{ie}, α_{ei}, α_{ii} are the "synaptic weights"; and $S(\cdot)$ is a nonlinear saturating function similar in form to $m_\infty(V)$.

7.3 Understanding Dynamics via Phase Plane Analysis

While an experimenter typically can measure membrane potential, it is usually impossible to monitor other dynamic variables, such as ionic currents, during nonclamped activity. For a theoretical model, we must explicitly compute the time courses of all dependent variables; we can then compare the time courses of the different dynamic variables and identify their contributions and temporal relationships. A valuable way to view the response of multiple variables and their relationship to physiological functions at the same time is by phase plane profiles, that is, curves of one dependent variable against another. Moreover, such plots allow us also to geometrically represent and interpret aspects of the model (e.g., activation curves) along with the response trajectories. At a glance, we can see whether the model has one or multiple steady states, which stimuli might invoke switching between states, and where these steady states lie in relation to activation and current-voltage (I-V) characteristics. While the phase plane view provides a full description for two-variable models, judicious two-dimensional projections from phase spaces of higher-order systems can yield some of these same insights.

Phase plane analysis was used effectively by FitzHugh (1960, 1961, 1969) to understand various aspects of the HH equations and the two-variable FitzHugh-Nagumo model. (FitzHugh 1969 also defines some basic mathematical terminology of nonlinear dynamics and supplements our presentation; for additional mathematical introduction, see also Edelstein-Keshet 1988 and Strogatz 1994.)

7.3.1 The Geometry of Excitability

We begin by considering the Morris-Lecar model (1981), in the case that there is a unique rest state and a thresholdlike behavior for action potential generation. Figure 7.1A shows the V responses to brief current pulses of different amplitudes. The peak V is graded, but the variation occurs over a very narrow range of stimuli; in this case, as in the standard HH model, the threshold phenomenon is not discrete, but rather, steeply graded. In figure 7.1B, these same responses are represented in the V-w plane. The solution path in the space of dependent variables is called a "trajectory," and direction of motion along a trajectory is often indicated by an

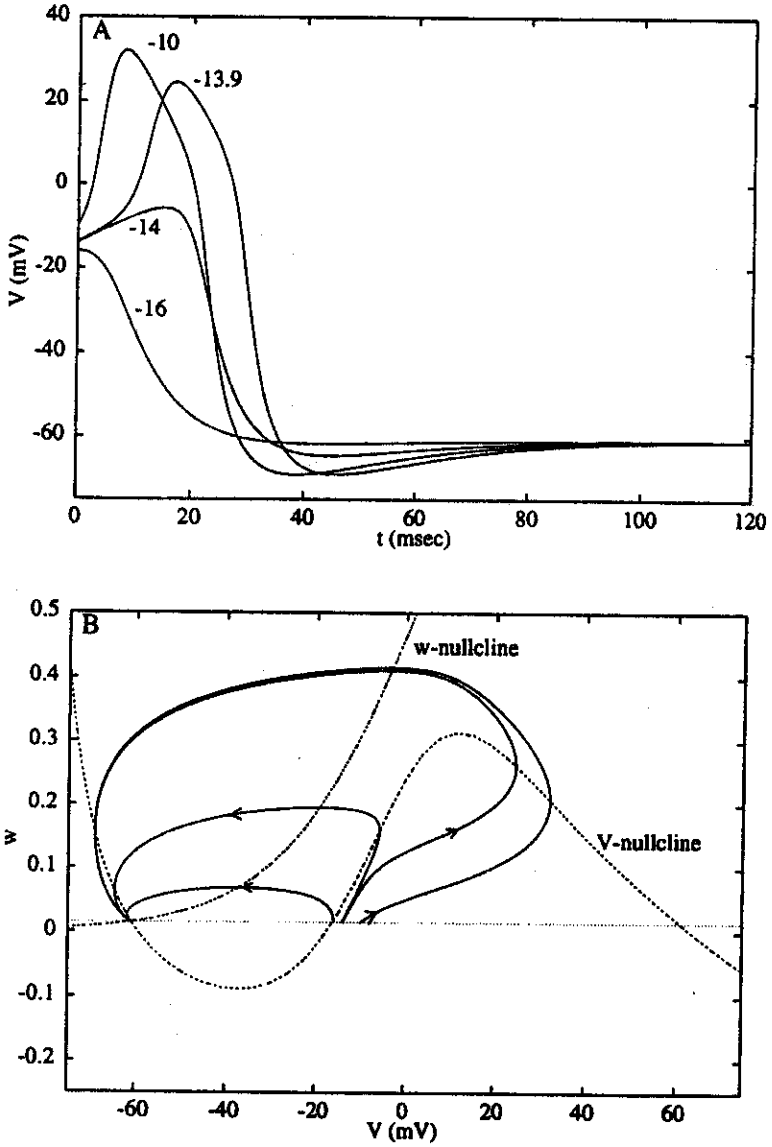

Figure 7.1
Response of the Morris-Lecar excitable system, eqs. 7.4–7.6, to a brief current pulse. For these parameters (see appendix A), the system has a unique stable rest state, $\bar{V} = -61\,\text{mV}$, $\bar{w} = .015$. The line $w = \bar{w}$ is shown lightly dashed. Four different stimuli lead to an instantaneous displacement of V from $\bar{V}$ to V_0 (values of V_0 are shown alongside the curves in panel A). Panel A shows the time course of the voltage. Notice that intermediate responses are possible with some stimuli: the threshold is graded; firing occurs with finite latency. Panel B shows trajectories in the V-w phase plane; nullclines are shown dashed and intersect only once. The effect of a stimulus is to displace the initial condition horizontally from rest.

arrowhead. In figure 7.1B, the flow is generally counterclockwise. All the trajectories shown here ultimately lead to the rest point: $V = \bar{V}, w = \bar{w} = w_\infty(\bar{V})$. The rest state is said to be "globally attracting." Each trajectory has a unique initial point, a horizontal displacement from the rest point corresponding to instantaneous depolarization by a brief current pulse. A trajectory's slope conveys the relative speed of w to V; thus a shallow slope means V is changing faster (see next paragraph). The trajectory of an action potential shows the following features: an upstroke with rapid increase in V (trajectory is moving rightward with little vertical component) and then the transient depolarized plateau with the delayed major increase in w, corresponding to the slower opening of K^+ channels. When w is large enough, the abrupt downstroke in V occurs—the trajectory moves leftward, nearly horizontal, as V tends toward V_K. Finally, as w decreases (the potassium channels close), the state point returns to rest with a slow recovery from hyperpolarization.

In the phase plane, the slope of a trajectory at a given point is dw/dV, which is simply the ratio of dw/dt to dV/dt, and these quantities are evaluated from the right-hand sides of the differential equations (eqs. 7.4–7.5). (The program XPP has a command to plot short vectors that indicate the flow pattern generated by the equations. This allows a global view of the flow without having to compute the trajectories. The program also computes nullclines, defined next.) Thus a trajectory must be vertical or horizontal where $dV/dt = 0$ or $dw/dt = 0$, respectively. The conditions

$$0 = -\bar{g}_{Ca} m_\infty(V)(V - V_{Ca}) - \bar{g}_K w(V - V_K) - \bar{g}_L(V - V_L) + I \tag{7.9}$$

$$0 = \phi \frac{[w_\infty(V) - w]}{\tau_w(V)} \tag{7.10}$$

define curves, the V and w nullclines, which are shown dashed in figure 7.1B. This provides a geometrical realization for where V and w can reach their maximum and minimum values along a trajectory in the V-w plane (notice how the trajectories cross the nullclines either vertically or horizontally in figure 7.1B). The w nullcline is simply the w activation curve, $w = w_\infty(V)$. The V nullcline, from eq. 7.9, corresponds to V and w values at which the instantaneous ionic current plus applied current is zero; below the V nullcline, V is increasing and above it, V is decreasing. The cubic-like shape seen here reflects the N-shaped *instantaneous I-V relation*, $I_{ion}(V, w)$ versus V with w fixed (eq. 7.6), typical of excitable membrane models in which the V-gated channels carrying inward current activate rapidly. From another viewpoint, motivated by the slower time scale of w, suppose we fix w, say, at a moderate value. Then the three points on the V nullcline at this w correspond to three pseudo–steady

states; at the low-V state, small outward and inward currents cancel while at the high-V state, both currents are larger but are again in balance. These states are transiently visited during the plateau phase and the return-to-rest phase of an action potential. Notice how the trajectory is near the right and left branches of the V nullcline during these phases.

If ϕ were smaller still, then the phase plane trajectories (except when near the V nullcline) would be nearly horizontal (because dw/dV would be small); the action potential trajectory during the plateau and recovery phases would essentially cling to, and move slowly along, either the right or left branch of the V nullcline. The downstroke would occur at the knee of the V nullcline. The time course would be more like that of a cardiac action potential. Also, in the case of smaller ϕ, the threshold phenomenon would be extremely steep; the middle branch of the V nullcline would act as an approximate separatrix between sub- and superthreshold initial conditions. In contrast, for larger ϕ, the response amplitude is more graded. This theoretical conclusion led Cole, Guttman, and Bezanilla (1970) to demonstrate experimentally that, at higher temperatures, the action potential for squid axon does not behave in an all-or-none manner.

We note that phase plane methodology applies to autonomous systems, whose equations have no explicit time dependence and whose nullclines and flow field therefore do not change with time. (This would not be the case if, for example, I were periodic in t; periodic stimuli will be covered later.) The phase plane method extends, however, to cases where a step change in a parameter occurs. At the time a parameter's value jumps, the nullclines would change instantaneously, but not the present location of V and w. FitzHugh (1961) uses this trick to interpret anodal break excitation, and Somers and Kopell (1993) have used this to analyze the behavior of coupled Morris-Lecar oscillators when ϕ is very small.

7.3.2 Oscillations Emerging with Nonzero Frequency

In the phase plane treatment, the rest state of the model is realized as the intersection of the two nullclines; such steady-state solutions are also referred to as singular or equilbrium points. From the geometrical viewpoint, one sees how different parameter values could easily lead to multiple singular points—by changing the shapes and positions of the nullclines. In figure 7.1, the unique singular point is attracting. Technically, we say it is asymptotically stable, that is, for any nearby initial point the solution tends to the singular point as $t \to \infty$. In general, the local stability of a singular point can be determined by a simple algebraic criterion (Edelstein-Keshet 1988; Strogatz 1994). The procedure is to linearize the differential equations, evaluate the partial derivatives at the singular point (this matrix of partial derivatives is

called the Jacobian), and to determine whether the exponential solutions to this constant coefficient system have any growing modes. If so, then the singular point is unstable; if all modes decay, then it is stable. For eqs. 7.4–7.6, the linearized equations that describe the behavior of small disturbances, $V \approx \bar{V} + x$, $w \approx \bar{w} + y$, from the singular point are

$$\frac{dx}{dt} = ax + by \tag{7.11}$$

$$\frac{dy}{dt} = cx + dy, \tag{7.12}$$

where

$$a = -\frac{\partial I_{ion}(V, w)}{\partial V} \tag{7.13}$$

$$b = -\frac{\partial I_{ion}(V, w)}{\partial w} \tag{7.14}$$

$$c = \frac{\phi}{\tau_w} \frac{dw_\infty}{dV} \tag{7.15}$$

$$d = -\frac{\phi}{\tau_w}. \tag{7.16}$$

Solutions are of the form $\exp(\lambda_1 t)$, $\exp(\lambda_2 t)$, where $\lambda_{1,2}$ are the eigenvalues of the Jacobian matrix in eqs. 7.11–7.12; they are roots of the quadratic

$$\lambda^2 - (a + d)\lambda + (ad - bc) = 0. \tag{7.17}$$

For the parameters of figure 7.1, the two eigenvalues are both real and negative.

As parameters are varied, the singular point may lose stability. In our example, the rest state could then no longer be maintained and the behavior of the system would change—it may fire repetitively or tend to a different steady state (if a stable one exists). Let us consider the effect of a steady applied current and ask how repetitive firing arises in this model. We will apply linear stability theory to find values of I for which the steady state is unstable. First, we note that for eqs. 7.4–7.6, and for nerve membrane models of the general form of eqs. 7.1–7.2, a steady-state solution $\bar{V}$ for a given I must satisfy $I = I_{ss}(\bar{V})$, where $I_{ss}(V)$ is the steady-state I-V relation of the model given by

$$I_{ss}(V) = I_{ion}(V, w_\infty(V)). \tag{7.18}$$

If I_{ss} is N-shaped, there will be three steady states for some range of I. If however, I_{ss} is monotonic increasing with V, as in the case of figure 7.1, then there is a unique $\bar{V}$ for each I; moreover, $(\bar{V}, \bar{w})$ cannot lose stability by having a single real eigenvalue pass through zero. Destabilization can only occur by a complex conjugate pair of eigenvalues crossing the axis $Re\,\lambda = 0$ as I is varied through a critical value I_1. At such a transition, a periodic solution to eqs. 7.4–7.6 is born—and we have the onset of repetitive activity. This solution, for I close to I_1, is of small amplitude and frequency proportional to $Im\lambda$. Emergence of a periodic solution in this way is called a Hopf bifurcation (Edelstein-Keshet 1988; Strogatz 1994).

From eqs. 7.11–7.12, or eq. 7.17, we know that $\lambda_1 + \lambda_2 = a + d$. Thus loss of stability occurs for the I whose corresponding $\bar{V}$ satisfies

$$\frac{\partial I_{ion}(V, w)}{\partial v} + \frac{\phi}{\tau_w} = 0. \tag{7.19}$$

The first term here is the slope of the instantaneous I-V relation and the second is the rate of the recovery process; this condition also applies approximately to the HH model (Rinzel 1978). From eq. 7.19 we conclude that loss of stability occurs: (1) only if the *instantaneous I-V relation* has negative slope at $\bar{V}$; (2) when the destabilizing growth rate of V from this negative resistance just balances the recovery rate; and (3) only if recovery is sufficiently slow, i.e. if ϕ is small (low "temperature"). In figure 7.2A, $\bar{V}$ is plotted versus I (this is the *steady-state I-V relation*, but shown as V against I) and the region of instability is shown dashed.

Figure 7.2A also shows the maximum and minimum values of V for the oscillatory response. Just as a singular point can be unstable, so, too, can a periodic solution (Strogatz 1994); unstable periodics are indicated by open circles. Here we see that the small amplitude periodic solution born at $I = I_1 = 93.85\,\mu A/cm^2$ from the loss in stability of $\bar{V}$ is itself unstable; it would not be directly observable. (In the phase plane, but not generally for higher-order systems, an unstable periodic orbit can be determined by integrating backward in time.) Note that solutions along this branch depend continuously on parameters and they gain stability at the turning point or knee at $I = I_v = 88.3\,\mu A/cm^2$. A stable periodic solution is called a "limit cycle." The upper branch (solid) corresponds to the limit cycle of observed repetitive firing. The frequency increases with I over most of this branch (figure 7.2B). At sufficiently large I, repetitive firing ceases (depolarization block) as $\bar{V}$ regains stability at $I = I_2 = 212\,\mu A/cm^2$. This figure is referred to as a "bifurcation diagram"; it depicts steady-state and periodic solutions, and their stability, as functions of a parameter

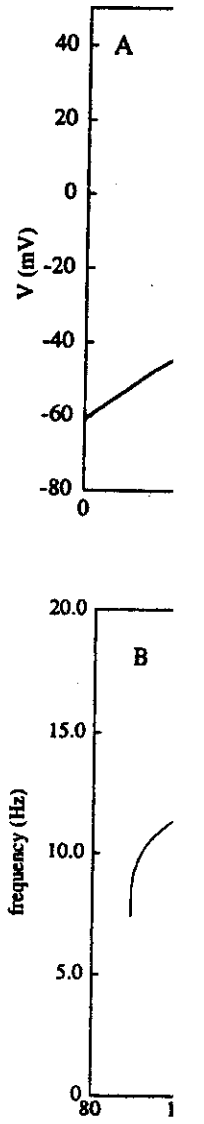

Figure 7.2
Repetitive firing ir
steady-state voltag
minimum voltage
branch of periodi
$I = I_2 = 212\,\mu A/c$
with the stable bra
$215\,\mu A/cm^2$. For t
that the frequency
bounded away fro

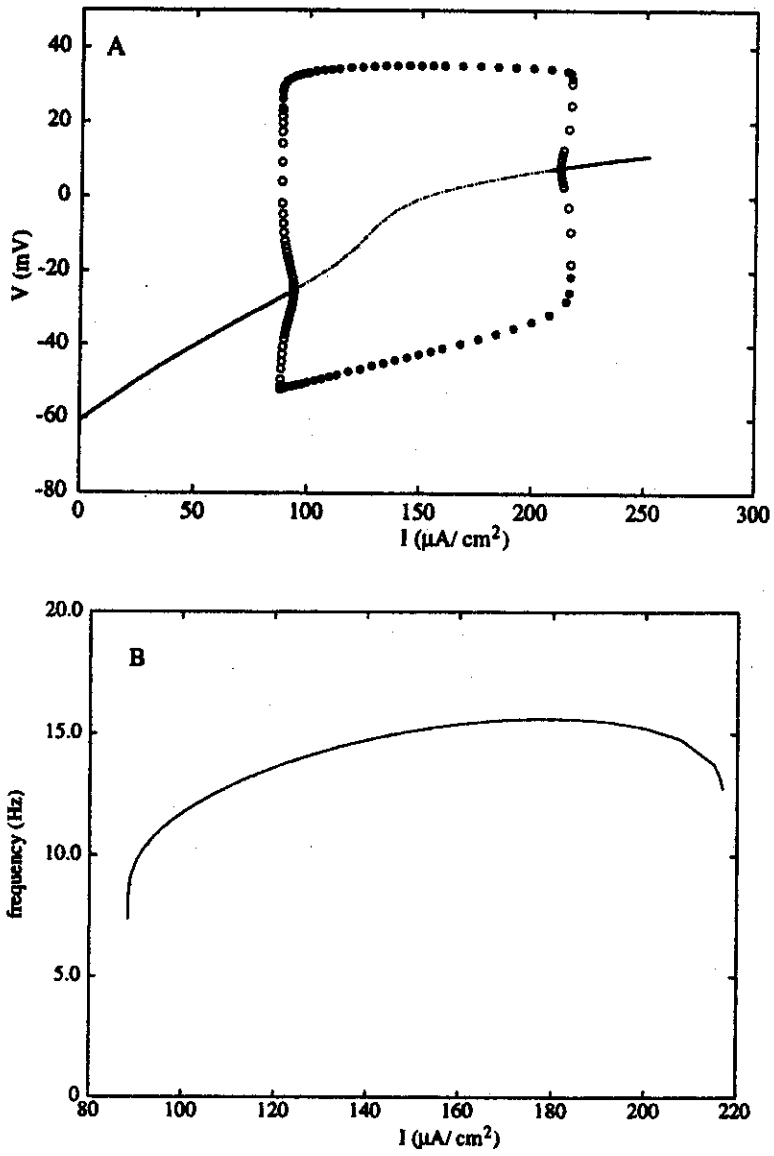

Figure 7.2
Repetitive firing in the Morris-Lecar model for steady current. Bifurcation diagram in panel A shows the steady-state voltage $\bar{V}$ versus I (thin lines; stable are solid, unstable are dashed) and the maximum and minimum voltage for periodic solutions shown as filled (stable) and unfilled (unstable) circles. The unstable branch of periodic solutions meets the branch of steady-state oscillations at $I = I_1 = 94\,\mu A/cm^2$ and $I = I_2 = 212\,\mu A/cm^2$ (Hopf bifurcation points). The unstable branch of periodic solutions coalesces with the stable branch of periodic solutions at $I = I_v = 88\,\mu A/cm^2$. A similar coalescence occurs near $I = 215\,\mu A/cm^2$. For these parameters, the steady-state I-V curve is monotonic. Furthermore, panel B shows that the frequency (plotted in Hz, and only for the stable limit cycles) as a function of current is always bounded away from zero. Parameters are as figure 7.1.

and it shows where one branch *bifurcates* (from the Greek word for branch) from another. Bifurcation theory allows one to characterize solution behavior analytically in the neighborhood of bifurcation points; for example, the frequency of the emergent oscillation at the Hopf point is proportional to $|Im\lambda_{1,2}|$. When the Hopf bifurcation leads to unstable periodic solutions, i.e., when the emergent branch bends back into the parameter region where the steady state is stable, then the bifurcation is *subcritical* (i.e., a hard oscillation); if the opposite occurs, it is *supercritical.*

For a range of I values (between the knee, I_v and the Hopf bifurcation, I_1), our model exhibits *bistability*: a stable steady state and a stable oscillation coexist. Figure 7.3A illustrates the phase plane profile in such a case; a periodic response here appears as a closed orbit. There is a stable fixed point shown as the intersection of the two nullclines and a stable periodic orbit (labeled SPO). The two attractors are separated by an unstable periodic orbit (UPO). Initial values inside the unstable orbit tend to the attracting steady state, while initial conditions outside of it will lead to the limit cycle of repetitive firing. A brief current pulse, whose phase and amplitude are in an appropriate range, can switch the system out of the oscillatory response back to the rest state. Such behavior has been seen for many models and observed, for example, in squid axon membrane (Guttman, Lewis, and Rinzel 1980). In figure 7.3B, two 30 $\mu A/cm^2$ current pulses 5 msec in duration are given, at $t = 100$ msec and then at $t = 470$ msec. The first pulse switches the membrane from rest to repetitive firing, while the second pushes the membrane back to rest. This bistable behavior is critical for the occurence of bursting oscillations when a very slow conductance is added to the model.

7.3.3 Oscillations Emerging with Zero Frequency

The Hopf bifurcation is one of a few generic mechanisms for the onset of oscillations in nonlinear differential equation models. In that case, the frequency at onset of repetitive activity has a well-defined, nonzero minimum. In contrast, some membranes and models (see, for example, Connor, Walter, and McKown 1977) exhibit zero (i.e., arbitrarily low) frequency as they enter the oscillatory regime of behavior; Rall's model (Goldstein and Rall 1974) also behaves this way. A basic feature in such systems is that I_{ss} versus V is N-shaped rather than monotonic, as in the previous section. For eqs. 7.4–7.6, this occurs if the V dependence of K^+ activation is translated rightward (see appendix A, and note value of V_3), so that the inward component of I_{ss} dominates over an intermediate V range. Thus, for some values of I, below the repetitive firing range, there are three singular points in the phase plane and the system is excitable. We discuss this case first. In figure 7.4B, we see the nullclines

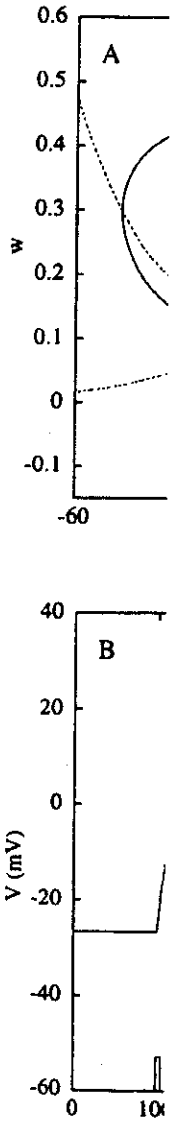

Figure 7.3
Bistability for ste
parameters as in
tion point, I_1, anc
the nullclines) an
shown in panel A
brief appropriatel

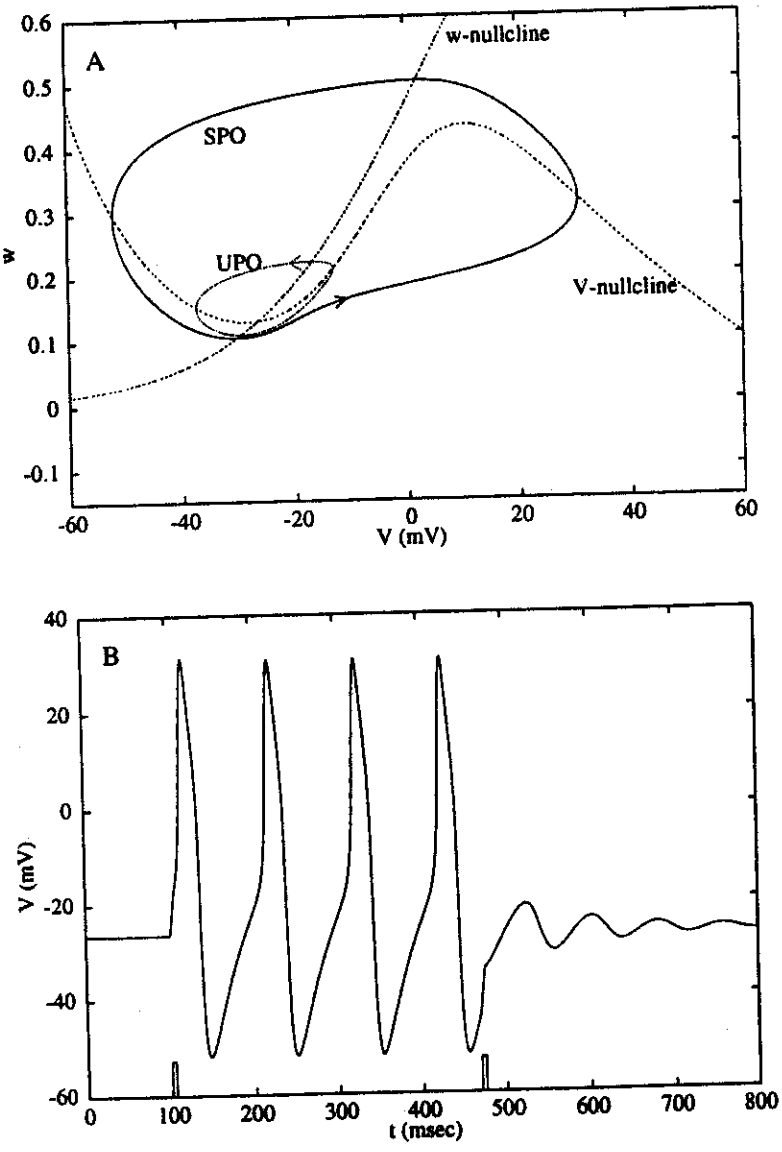

Figure 7.3
Bistability for steady current near the threshold for repetitive firing for the Morris-Lecar model with parameters as in figure 7.1 and $I = 90\,\mu A/cm^2$. In this region, where I is between the first Hopf bifurcation point, I_1, and the "knee," I_ν, there are two stable states (cf figure 7.2): a rest state (the intersection of the nullclines) and a stable oscillation (SPO) separated by an unstable periodic solution (UPO). This is shown in panel A. Panel B demonstrate switching from rest to oscillation and then back to rest for two brief appropriately timed depolarizing current pulses.

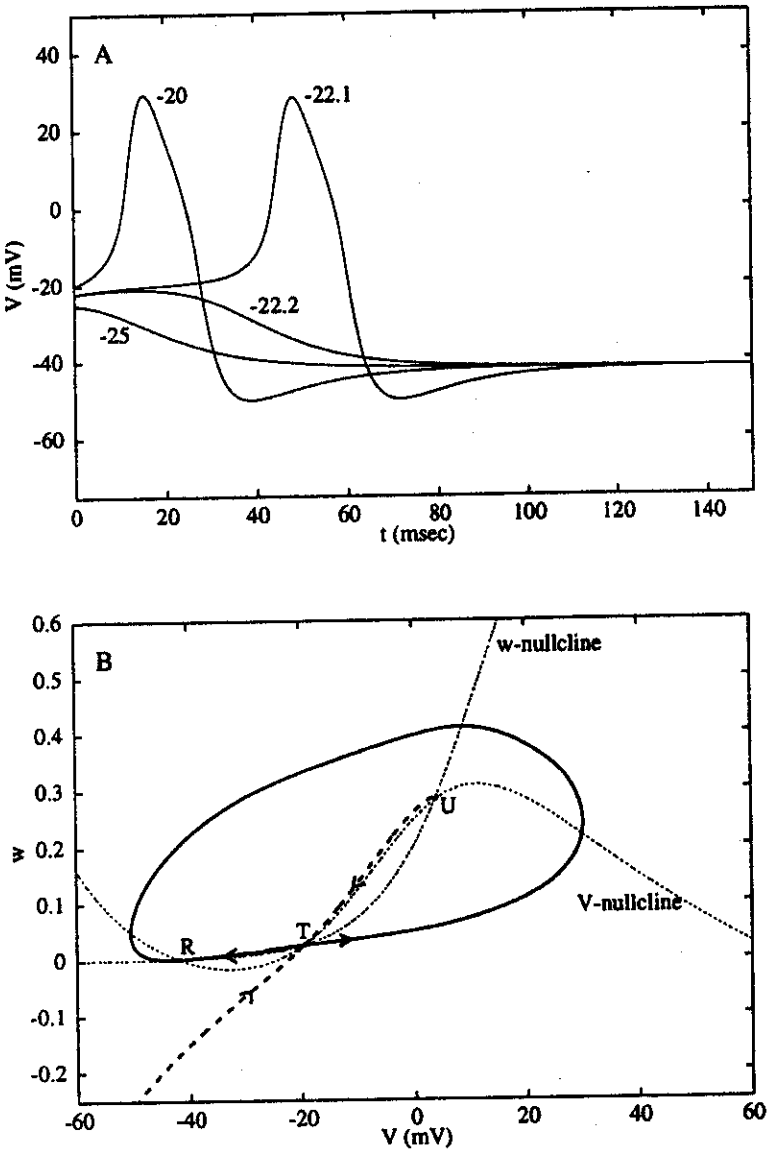

Figure 7.4
Excitability with three steady states and a distinct threshold; the response of the membrane to a brief current pulse from the stable rest state. Four different stimuli result in a displacement of V from $\bar{V}$ to V_0 (values of V_0 are given alongside the curves in panel A). (A) Time course of the voltage for $I = 30\,\mu A/cm^2$. (B) Phase plane for the dynamics illustrated in panel A. Nullclines intersect at three places: (1) R a stable rest state, (2) T, a saddle point threshold, and (3) U an unstable node. The thick solid line shows the unstable manifold for the saddle point; here, unstable refers to movement in opposing directions away from T (indicated by arrowheads). The manifold's two branches lead to the stable rest state and form a smooth loop in phase space. The heavy dashed line shows the stable manifold for the saddle point (arrowheads pointing toward T). Any initial conditions to the left of this manifold decay to rest. Initial conditions to the right lead to an action potential before returning to rest. Parameters are as in figure 7.1, except $\bar{g}_{Ca} = 4\,mS/cm^2$, $V_3 = 12\,mV$, $V_4 = 17.4\,mV$, $\phi = 1/15$.

intersecting thr
are the stable
stable spiral (U
attracting rest
larger stimuli l
The phase plan
distinct thresho
this, we note th
ries (bold dash
matrix; togethe
eigenvalue are
these are the u
folds.) The stab
distinguishes su
the threshold s
threshold respo
not exactly on)
singular point (
w_R, then there
present example
the line $w = w_R$

The action p
which passes ar
a trajectory joi
branch of the u
rest point. This
outside it—thus
not find graded

This case als
there are three s
is unstable. In f
none of which i

Next, we tune
we know that t
creases, and the
means that the
"saddle node bi
loop, a limit cyc

intersecting three times. As determined by linear stability theory, the singular points are the stable rest state (**R**), and unstable saddle point threshold (**T**), and an unstable spiral (**U**). The system is excitable, with the lower state being a globally attracting rest state: initial conditions near R lead to a prompt decay to rest, while larger stimuli lead to an action potential—a long trajectory about the phase plane. The phase plane portrait moreover reveals that this case of excitability indeed has a distinct threshold which is due to the presence of the saddle point, T. To understand this, we note that associated with the saddle are a unique pair of incoming trajectories (bold dashed lines) corresponding to the negative eigenvalue of the Jacobian matrix; together, these represent the *stable manifold.* Corresponding to the positive eigenvalue are a pair of trajectories (bold lines) that enter the saddle as $t \to -\infty$; these are the *unstable manifold.* (XPP has a command that generates these manifolds.) The stable manifold defines a separatrix curve in the phase plane that sharply distinguishes sub- from superthreshold initial conditions. For initial conditions near the threshold separatrix, there is a long latency before a firing or decaying subthreshold response (see figure 7.4A). This is because the trajectory starts close to (but not exactly on) the stable manifold and thus the solution comes very near the saddle singular point (where it moves very slowly) before taking off. If w is started at rest, w_R, then there is a unique value of $V = V_T$ (between -22.1 and $-22.2\,\mathrm{mV}$ in the present example) called the "voltage threshold," where the stable manifold intersects the line $w = w_R$.

The action potential trajectory follows along the unstable manifold (bold lines), which passes around the unstable spiral and eventually tends to the rest point. Such a trajectory joining two singular points is called a "heteroclinic orbit." The other branch of the unstable manifold is also a heteroclinic orbit from the saddle to the rest point. This heteroclinic pair forces any trajectory that begins outside it to remain outside it—thus preserving the amplitude of the action potential. In this case we do not find graded responses for any brief current pulses from the rest state.

This case also provides a counterexample to the common misconception that if there are three steady states, then the "outer" two are stable, while the "middle" one is unstable. In fact, in some parameter regimes this model has three singular points, none of which is stable.

Next, we tune up I and ask when repetitive firing occurs. Because I_{ss} is N-shaped, we know that the lower and middle values of $\bar{V}$ move toward each other as I increases, and there is a critical value I_1 where they meet. In the phase plane, this means that the rest point and the saddle coalesce and then disappear; this is called a "saddle node bifurcation." Moreover, the heteroclinic pair become a single closed loop, a limit cycle, which for I just above I_1 has very long period (figure 7.5). Thus,

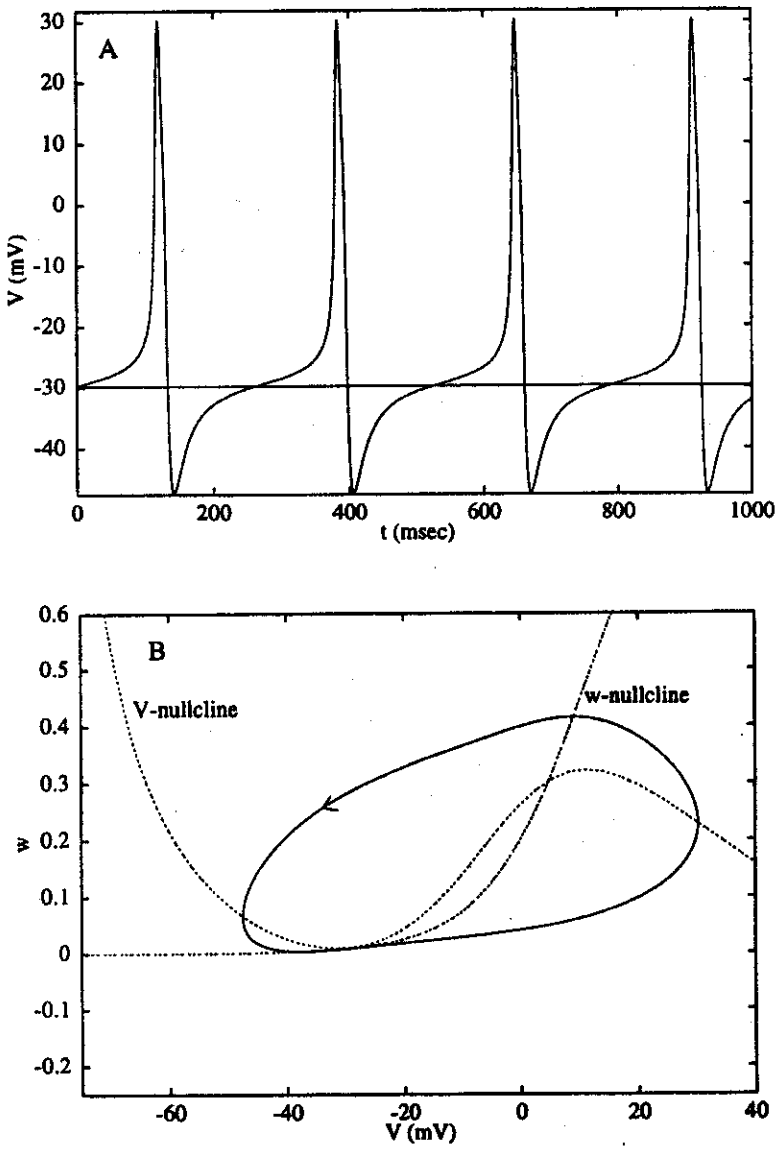

Figure 7.5
Onset of repetitive firing with arbitrarily low frequency for a constant current, $I = 40.76\,\mu A/cm^2$ shows an oscillation with a period of about 220 msec. Panel A shows the voltage time course and panel B shows the phase plane. Note the "narrow channel" between the two nullclines near -30 mV, which accounts for most of the oscillation period (see Rinzel and Ermentrout 1989). Parameters are as in figure 7.4.

in this parameter regime, the transition to repetitive firing is marked by arbitrarily low frequency (figure 7.6B). For I near the critical current, the frequency is proportional to $\sqrt{I - I_1}$ (Strogatz 1994). When $I = I_1$, the limit cycle has infinite period; it is called a "saddle node loop" or SNIC (saddle node on an invariant circle). Generally, an infinite period limit cycle is called a "homoclinic orbit," one that begins and ends at a singular point. The saddle node loop is one type of homoclinic orbit; we will encounter another type in the next section. This type of zero-frequency onset is generic and occurs over a range of parameters. Changing another parameter will typically lead to a smooth change in I_1. We emphasize that this mechanism allows arbitrarily low firing rates without relying on channel gating kinetics, which are necessarily slow. Such low rates have been associated with the inactivating potassium A-type current (Connor, Walter, and McKown 1977), although the underlying mathematical structure of the saddle node loop does not, of course, require an A-current (Rush and Rinzel 1995). We have found the fast spike dynamics in several recent models (e.g., Traub et al. 1991) for cortical pyramidal cells to have this same zero-frequency onset of repetitive firing (unpublished observations by the authors). The value I_1 is determined by evaluating I_{ss} at the value of V for which $\partial I_{ss}/\partial v = 0$, and this latter condition is equivalent to having the determinant $ad - bc$ of the Jacobian matrix equal zero.

The global picture of repetitive firing is shown in the bifurcation diagram of figure 7.6A, with frequency versus I in figure 7.6B. The branch of steady states (unstable shown dashed) form the S-shaped curve, and the oscillatory solutions are represented by the forked curve whose open end begins at $I = I_1$. As I increases beyond I_1 the peak-to-peak amplitude on the stable (repetitive firing) branch decreases and the frequency increases. The family of periodic solutions terminates at $I = I_2$ via a subcritical Hopf bifurcation. Except for I in a small interval of this upper range, this system is monostable. Annihilation of repetitive firing, as in figure 7.3, cannot be carried out for I near I_1 in this case (although at the high-current end where there is bistability, annihilation can occur).

7.3.4 More Bistability

It is important to realize that the solution behavior we have described in our bifurcation diagrams depends on other parameters in the model. The temperature parameter ϕ is particularly convenient, with useful interpretative value for additional parametric tuning: it plays no role in I_{ss} and thus does not affect the values along the S-shaped curve of steady states in figure 7.6, or the corresponding curve in figure 7.2. The *stability* of a steady state does, however, depend on ϕ. As is seen from eq. 7.19,

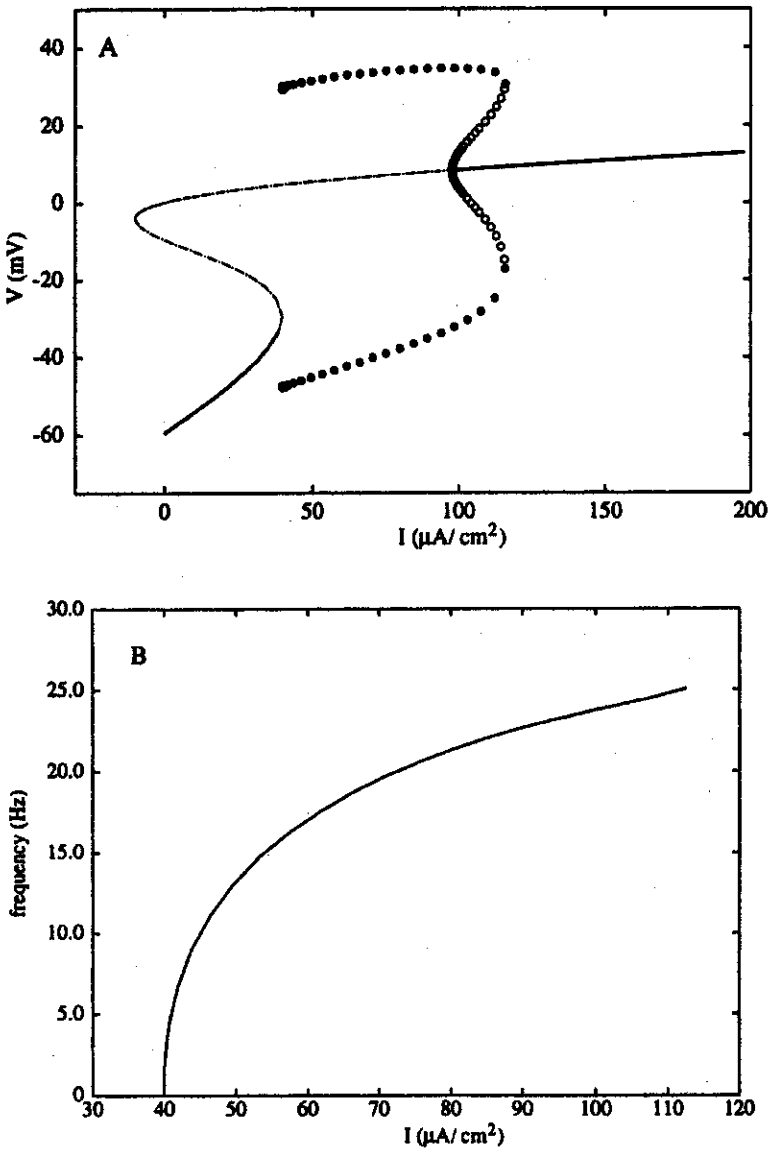

Figure 7.6
Multiple steady states and periodic orbits for a steady current when the I_{ss}–V relation is N-shaped. (A) Bifurcation diagram (line types as in figure 7.2A; parameters are as in figures 7.4–7.5). In spite of the coexistent states, the system is monostable for I between $I_1 = 40$, the turning point of the steady states, and $I_2 = 98$ where there is a Hopf bifurcation. Onset of repetitive firing at zero frequency occurs at $I = I_1$ where two fixed points coalesce. This corresponds to figure 7.4B when the unstable manifolds of the saddle point form a closed loop. The branch of periodic orbits has a turning point at $I = 116$ before terminating at the Hopf bifurcation point, $I = I_2$. All current values in μA/cm^2. (B) Frequency (in Hz) of stable branch of periodic orbits.

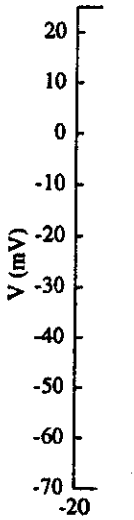

Figure 7.7
Bifurcatio
coalesce,
of the sta
solutions
homoclini
(2) a high
that of fig
Vertical li

when ϕ
steady s
Thus, fo
middle
kinetics
that the
only by
unstable
venientl
ences be
For i
and the
furcatio

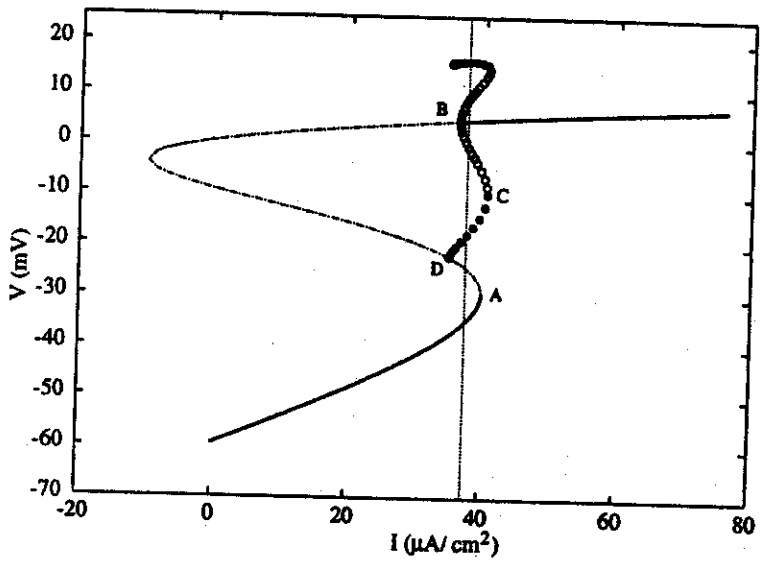

Figure 7.7
Bifurcation diagram (as in figure 7.6 but for $\phi = 0.23$). Point A shows where the two lower steady states coalesce, point B shows the Hopf bifurcation for the upper steady state, point C shows the coalescence of the stable and unstable periodic branches, and point D shows where the branch of stable oscillatory solutions terminates on the branch of saddle points (not on the knee, as in figure 7.6) at a saddle loop homoclinic. For currents between points B and A, there are three stable states: (1) a low-voltage rest state, (2) a high-voltage rest state, and (3) an oscillatory state. Note that the steady-state branch is identical to that of figure 7.6; ϕ only affects the stability of the steady states and the behavior of the periodic orbits. Vertical line at $I = 37.5\,\mu A/cm^2$ shows a current for which there are three stable states (cf. figure 7.8).

when ϕ is large, oscillatory destablization is precluded; Hopf bifurcation from a steady state only occurs when the time scale of w is slow compared to that of V. Thus, for large ϕ, both the upper and lower branches of the S-curve are stable; the middle branch is of course unstable. This system is bistable. In this large-ϕ limit, the kinetics of the K^+ system are so fast (essentially instantaneous, with $w = w_\infty(V)$) that the model reduces to one dynamic variable, V. Then stability is determined only by the slope of I_{ss}, with the two "outer" states being stable and the "middle" unstable. This simple example also shows that sometimes a model can be conveniently reduced to a lower dimension when there are significant time scale differences between variables.

For intermediate values of ϕ, the dynamics of both V and w influence stability, and the upper branch is unstable for a certain range of I. Figure 7.7 shows a bifurcation diagram analogous to that in figure 7.6A, in which the branch of steady

states is S-shaped and the stable rest state disappears at a turning point (point A). The high voltage equilibrium is stable for large currents but, as the current is reduced, loses stability at a subcritical Hopf bifurcation (point B). An unstable branch of periodic solutions emanates from the Hopf bifurcation point and then becomes stable at a turning point (C). Unlike figure 7.6A, however, this branch of stable periodic orbits (solid circles) does not terminate on the knee (point A) but instead on the unstable middle branch (point D on the diagram) as the current decreases to a critical value, I_D. Again the frequency of the limit cycle tends to zero for this branch, but not as the square root. Rather, the frequency is proportional to $1/|\log(I - I_D)|$ (Strogatz 1994). At the critical value of current, I_D, the closed orbit has infinite period; it is called a "saddle loop homoclinic orbit." Recall that the middle branch of solutions is a saddle point. One branch of the unstable manifold of this saddle point exits the singular point and returns via a branch of the stable manifold (compare figure 7.8A) and contrast this with the saddle node loop homoclinic in figures 7.4–7.6). For certain values of the current, this system is *tristable*, that is, it has three stable states. If I is chosen to lie between the I values for points B and C, then the lower branch still exists and is stable, the upper branch of equilibria is stable, and there is a stable periodic orbit. Figure 7.8A shows the phase plane for this case. The stable manifold for the saddle point (bold dashed trajectory) acts to separate the stable periodic orbit (SPO) from the lower rest state. The small unstable periodic orbit (UPO) separates the upper rest state from the stable periodic solution. As in figure 7.3B, we can use brief current pulses to switch between states. Figure 7.8B shows the effect of three 5 msec current pulses switching from the periodic orbit to the lower rest state, back to the periodic orbit, and then to the upper rest state. (Note that perturbations from the upper rest state decay very slowly.) The HH model, adjusted for higher than normal external potassium, exhibits similar multistable behavior (Rinzel 1985).

This example of coexistence between a depolarized limit cycle and a lower resting state is important because it also forms the basis for a general class of bursting phenomena.

7.4 Bursting and Adaptation: Spiking Dynamics with Slow Modulation

Many neurons exhibit much more complicated firing patterns than the simple repetitive firing we have described here. *Bursting*, the clustering of spikes followed by relative quiescence, is a common mode of firing in neurons and other excitable cells (see Wang and Rinzel 1995 for a brief review). Bursting cannot happen in two-variable

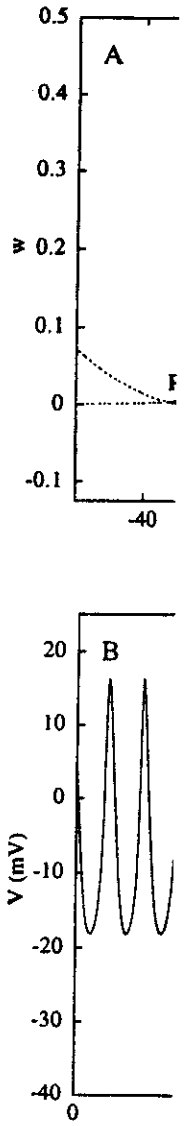

Figure 7.8
Multistability for . as in figure 7.7). P steady states: (1) a state (unlabeled). ' lower steady state stable manifold of and the stable per from the stable pc Starting on the sta pulse pushes it ba single brief curren though the opposi

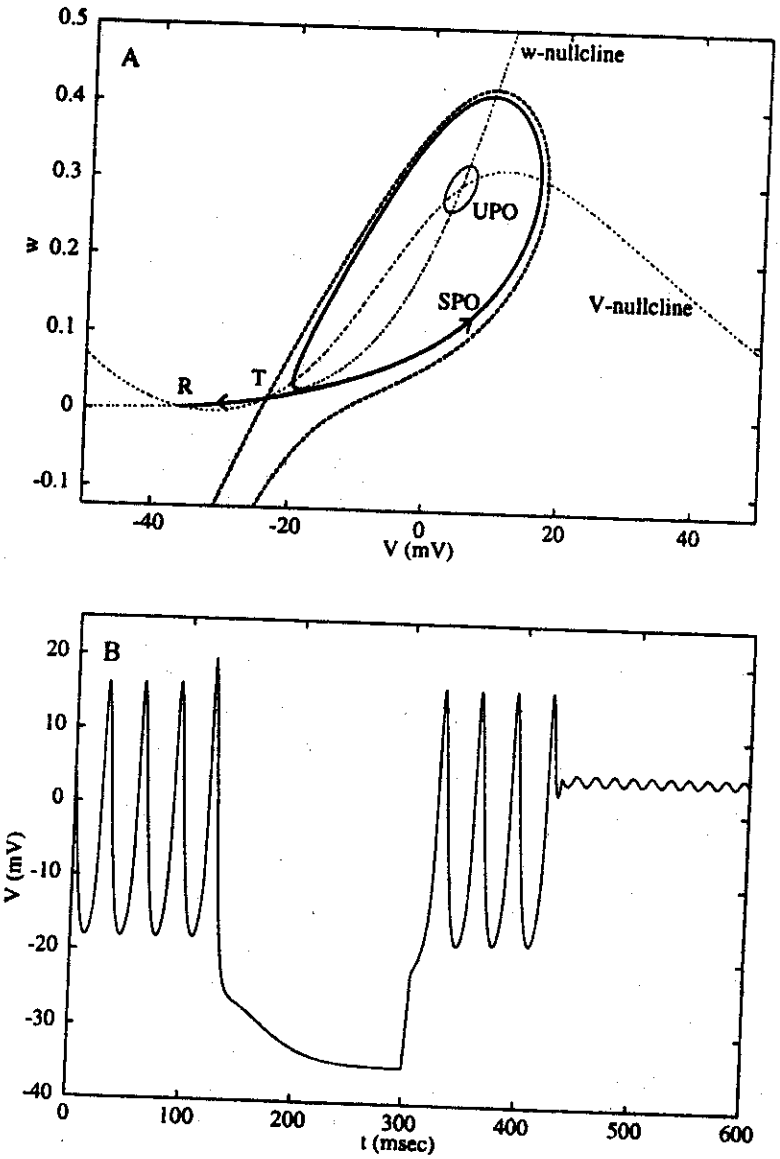

Figure 7.8
Multistability for a current between points B and A in figure 7.7 ($I = 37.5\,\mu A/cm^2$; other parameters are as in figure 7.7). Panel A depicts the V-w phase plane. The nullclines intersect at three places representing steady states: (1) a lower stable rest state (R), (2) an unstable saddle point (T), and (3) an upper stable rest state (unlabeled). The left branch of the unstable manifold of the saddle point (bold line) connects to the lower steady state. The right branch wraps around the stable periodic orbit (SPO). The branches of the stable manifold of the saddle point (bold dashed line) form a separatrix between the lower stable rest state and the stable periodic orbit. The unstable periodic orbit (UPO) separates the stable upper steady state from the stable periodic orbit. Panel B shows the effects of three successive depolarizing current pulses. Starting on the stable oscillation, the membrane is switched to the lower stable steady state. Another brief pulse pushes it back to the stable oscillation and a third pulse switches it to the upper steady state. No single brief current pulse can switch it from the lower steady state directly to the upper steady state, although the opposite transition is possible.

models. The slow modulation of spiking during a burst requires additional biophysical mechanisms and dynamic variables. Moreover, just from mathematical considerations, a slowly drifting spike trajectory that recurs would violate the rule that trajectories in the phase plane cannot cross. By adding a slow process to our idealized two-variable model, however, we can use it to understand bursting from a simple geometric point of view. In this treatment, a slow variable is first viewed as a parameter to describe the behavioral regimes of the fast spike-generating kinetics; the slow dynamics are then overlaid as the full system sweeps through regimes of spiking and quiescence. Unless we state otherwise, bursting for us will imply repetitive bursting.

7.4.1 Square-Wave Bursters

Consider in figure 7.7 the I interval between A and D. There is a stable rest state around $-35\,\mathrm{mV}$ and a stable (more depolarized) limit cycle. Suppose the current I slowly varies back and forth across this interval. Then because of the bistability, a hysteresis loop is formed, in which the membrane is alternately at rest and alternately firing repetitively. Such a loop provides a simple mechanism and geometric interpretation for *square-wave bursting*. Because the current I is externally imposed, however, this is forced rather than autonomous bursting. To achieve autonomous bursting, one could (as in Rinzel and Ermentrout 1989) redefine I as a dynamic dependent variable in such a way that I decreases when the membrane is depolarized and firing repetitively, and I increases when the membrane is resting. Although artificial, this example demonstrates the basic principle that (very) slow negative feedback and hysteresis in the fast dynamics underlie square-wave bursting. Many different ionic current mechanisms could likewise produce the slow negative feedback. For further illustration, we employ a calcium-dependent potassium current, analogous to that studied by others (see Wang and Rinzel 1995). We assume the current activates instantaneously in response to calcium and that the calcium-handling dynamics are slow. Thus we add to eq. 7.6 the current I_{K-Ca} given by

$$I_{K-Ca} = g_{K-Ca} z (V - V_K), \tag{7.20}$$

where g_{K-Ca} is the maximal conductance for this current and z is the gating variable with a Hill-like dependence on Ca (the near-membrane calcium concentration scaled by its dissociation constant for activating the gate, K_D):

$$z = \frac{Ca^p}{Ca^p + 1}. \tag{7.21}$$